Revista de Matemática: Teoría y Aplicaciones 2015 **22**(2) : 199–222
cimpa – ucr issn: 1409-2433 (Print), 2215-3373 (Online)

PRECISION OF GEOID APPROXIMATION AND GEOSTATISTICS: HOW TO FIND CONTINUOUS MAP OF ABSOLUTE GRAVITY DATA

PRECISIÓN DE LA APROXIMACIÓN GEOIDE Y GEOESTADÍSTICA: CÓMO ENCONTRAR UN MAPA CONTINUO DE DATOS DE GRAVEDAD ABSOLUTA

Hongzhi Song* Alexey Sadovski† Gary Jeffress‡

Received: 28/Aug/2013; Revised: 3/Oct/2014;
Accepted: 29/Oct/2014

---

*Conrad Blucher Institute for Surveying and Science, School of Engineering and Computing Sciences, Texas A&M University-Corpus Christi, United States. E-mail: hongzhi.song@tamucc.edu

†Department of Mathematics & Statistics, Texas A&M University-Corpus Christi, United States. E-mail: alexey.sadovski@tamucc.edu

‡Same address as/*Misma dirección que* H. Song. E-mail: gary.jeffress@tamucc.edu

Abstract

An accurate geoid model is needed for surveyors and engineers who require orthometric heights on a common datum, and environment scientists who require elevations relative to present sea level. Airborne gravity data has been collected by the National Geodetic Survey (NGS) under the Gravity for the Redefinition of the American Vertical Datum (GRAV-D) project and is available along the coasts of the Gulf of Mexico. For this study we obtained a set of absolute gravity data derived from full-field gravity at altitude/elevation. We used the data to derive free-air gravity anomalies to establish gravity on the geoid. For spatial interpolation we used the kriging method to estimate gravity on the geoid in any location and kriging of the difference between gravity on the ellipsoid of reference and the geoid. Various kriging methods were used for evaluation of errors calculated in this study. The mean precision of the predicted values is around 1.23 cm, a very good result for coastal regions, which traditionally have sparse gravity data sets.

Keywords: geoid; geospatial statistics; kriging; gravity; precision.

Resumen

Los agrimensores e ingenieros necesitan un modelo preciso del geoide ya que requieren alturas ortométricas de datos comunes, y los científicos del ambiente requieren de elevaciones reales del nivel del mar. La Encuesta Nacional Geodética (NGS por sus siglas en inglés) del proyecto Gravedad para la Redefinición del Datum Vertical Americano (GRAV-D, por sus siglas en inglés) ha recogido datos de gravedad en el aire para las costas del Golfo de México. Para este estudio obtuvimos un conjunto de datos de gravedad absoluta derivados de gravedad completa de campo en altitud/elevación. Usamos los datos para derivar anomalías de gravedad de aire libre con el fin de establecer gravedad en el geoide. En la interpolación espacial usamos el método de kriging para estimar la gravedad en el geoide en cualquier lugar y kriging de la diferencia entre gravedad del elpsoide de referencia y el geoide. Varios métodos de kriging se usaron para evaluar los errores calculados en este estudio. La precisión media de los valores predicho ande alrededor de 1.23 cm, un resultado muy bueno para regiones costeras, que tradicionalmente tienen conjuntos de datos de gravedad dispersos.

Palabras clave: geoide; estadística geoespacial; kriging; gravedad; precisión.

Mathematics Subject Classification: 91B72, 62J99, 62J05.

1 Introduction

It is very popular to use satellite based positioning techniques, especially the US global positioning system (GPS) for geodetic and surveying work. Using GPS can be quicker and easier than using leveling in determining elevations; however, there is a much faster and more economical approach, which is to use geoid models associated with modern satellite technology. There is a need for more precise geoid models, especially in coastal regions to be better prepared for sea level rise and to improve coastal resilience.

Gravity is continuously changing, which reflects the results of Earth's dynamic phenomena, including tropical storms, hurricanes, earthquakes, yearly tides, and severe variations in the atmosphere density, etc. In principle, there is a need for gravity g at every point of the Earth's surface. However, having gravity data provided everywhere on the Earth is totally impossible in reality. To predict values of a random unsampled area from a set of observations is needed. There are two common interpolation techniques used to produce a prediction of a random field [11]. One is least-square collocation, which is mainly used in geodesy; the other technique that is mainly used in geology and hydrology is called kriging. In this paper, we assume that the kriging method is a better approach for prediction of gravity based on the airborne data due to the flexibility derived from different modeling techniques. Another advantage of the kriging method is its ability to estimate a predicted error to assess the quality of a prediction.

2 Data

Data used in this paper is airborne gravity data of the Gravity for the Redefinition of the American Vertical Datum (GRAV-D) project which was released by NGS (`http://www.ngs.noaa.gov/GRAV-D`). Table 1 lists the nominal block characteristics, and details can be founded in *GRAV-D General Airborne Gravity Data User Manual*. Four blocks (Block CS01, CS02, CS03 and CS04) data (Figures 1 and 2) were chosen to be interpolated [4, 5].

The total sample size (four blocks together) is 389578 single point gravity values, with a range between 975480 mgal and 977490 mgal. Keep in mind, the standard gravity is 980665 mgal. The descriptive statistics of airborne gravity data is listed in upper right corner of Figure 3. Figure 4 shows the normal QQ plot of airborne gravity data. The airborne gravity

Table 1: Nominal block and survey characteristics.

Characteristic	Nominal Value
Altitude	20.000 ft ($\approx$ 6.3 km)
Ground speed	250 knots (250 nautical miles/hr)
Along-track gravimeter sampling	1 sample per second =128.6 m (at nominal ground speed)
Data line spacing	10 km
Data line length	400 km
Cross line spacing	40-80 km
Cross line length	500 km
Data minimum resolution	20 km

Source: GRAV-D Science Team [4, 5].

data was fixed by using free-air reduction and by the international gravity formula [7].

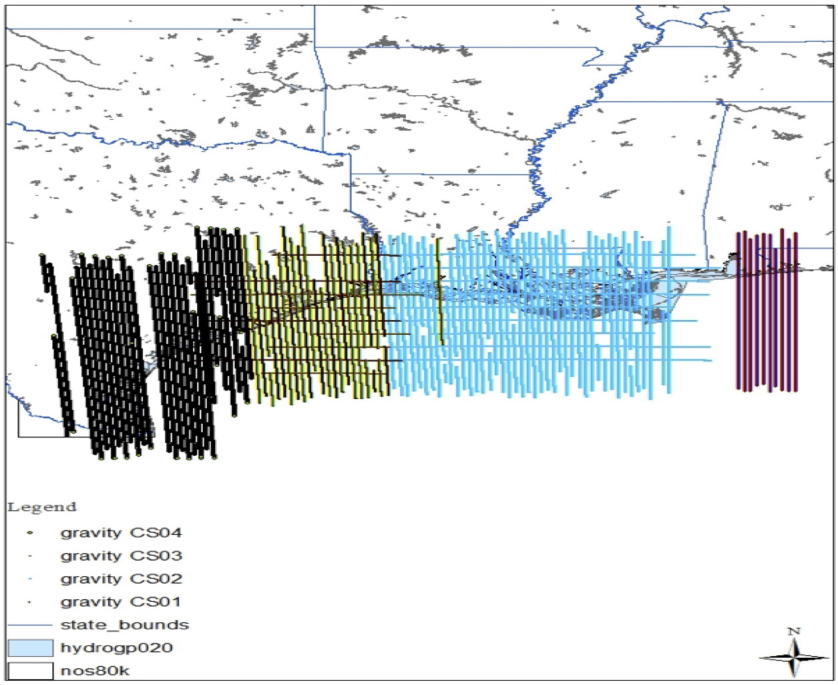

Figure 1: Tracks and locations of data of airborne gravity. Gravity data plotted by individual block from CS01 to CS04.

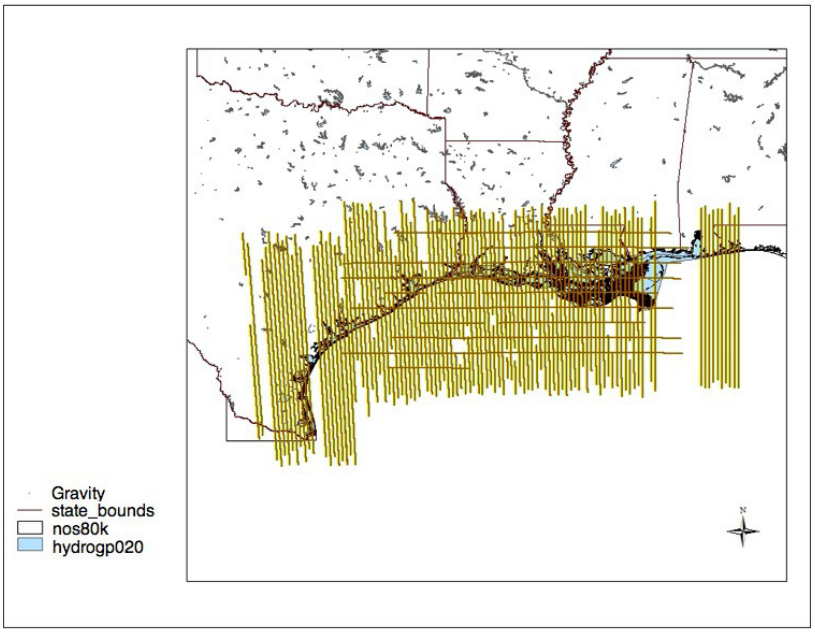

Figure 2: Tracks and locations of data of airborne gravity. Gravity data plotted by four blocks as a group.

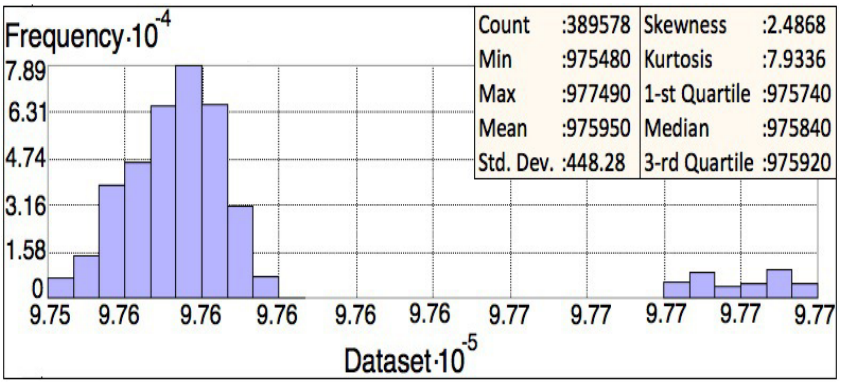

Figure 3: Frequency histogram with descriptive statistics for airborne gravity data (unit in mgal).

2.1 Free-air correction (FAC)

Topographic masses outside the geoid need to be removed by using different gravity corrections in order to determine the geoid. Using the Taylor

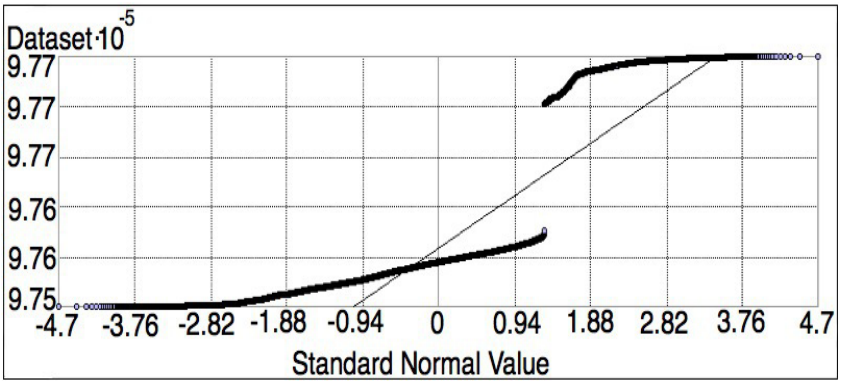

Figure 4: Normal QQ plot of airborne gravity data (unit in mgal).

series [6, 7], the gravity is reduced onto the geoid g_g and is calculated by

$$g_g = g_o - \frac{\partial g}{\partial H} H \tag{1}$$

where g_o is the observed gravity, and H is the elevation. $\frac{\partial g}{\partial H}$ is defined as free-air correction factor which is 0.3086 mgal/m. g_g presented in Figure 5, and the values ranged from 978960 mgal to 979470 mgal with a mean of 979230 mgal and standard deviation 105.79 mgal. Normality of sampling distribution is tested for determining the kriging methods to be used. In order to do so, skewness and kurtosis are tested within data of gravity values on the geoid (Figure 6). The skewness is -0.29, which is a slightly left skewed distribution. The values are more concentrated on the right of the mean. The kurtosis is 2.28, which is flattened more than a normal distribution with a wide peak (platykurtic). Points on the Normal QQ plot (Figure 7) also deviate from the reference line represented in black line.

2.2 The international gravity formula (IGF)

The international gravity formula estimates theoretical gravity change with latitude on the ellipsoid surface. Based on the Helmert theorem, there are several international gravity formulas. The difference of these IGFs is explained in Li and Götze [7]. IGF 1980 [7, 8] is used in this paper:

$$\gamma = 978032.7(1 + 0.0053024 \sin^2\phi - 0.0000058 \sin^2 2\phi) \tag{2}$$

where ϕ is the latitude; the unit of γ is mgal.

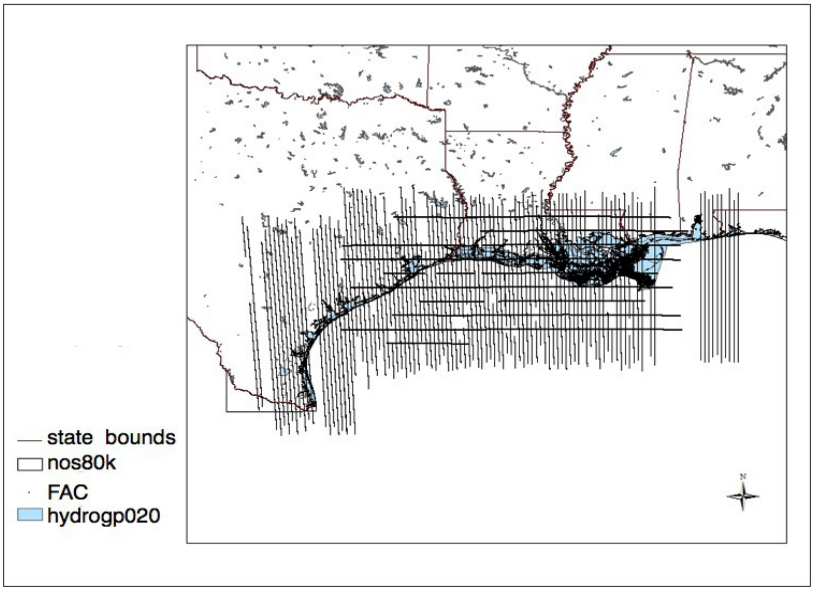

Figure 5: The airborne gravity reduced onto the geoid by free-air correction.

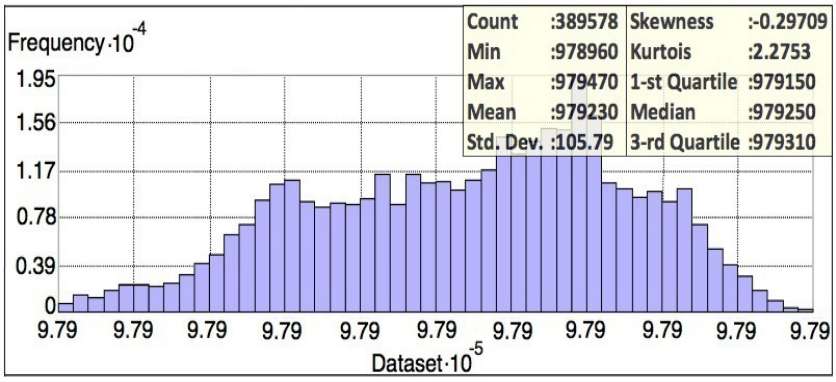

Figure 6: Frequency histogram with descriptive statistics for data of gravity on the geoid (unit in mgal).

The values of gravity on the ellipsoid ranged from 978970 mgal to 979450 mgal with a mean of 979240 mgal and standard deviation 106.43 mgal. More details about descriptive statistics are listed in upper right corner of Figure 8. Points on the Normal QQ plot (Figure 9) deviate from the reference line represented in black line.

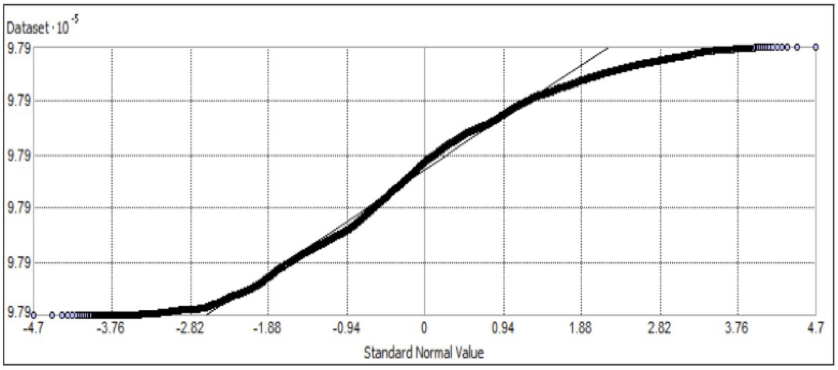

Figure 7: Normal QQ plot of gravity on the geoid data (unit in mgal).

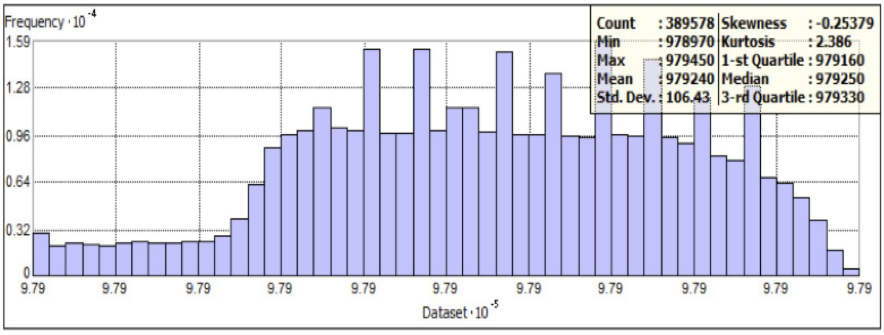

Figure 8: Frequency histogram with descriptive statistics for data of gravity on the ellipsoid (unit in mgal).

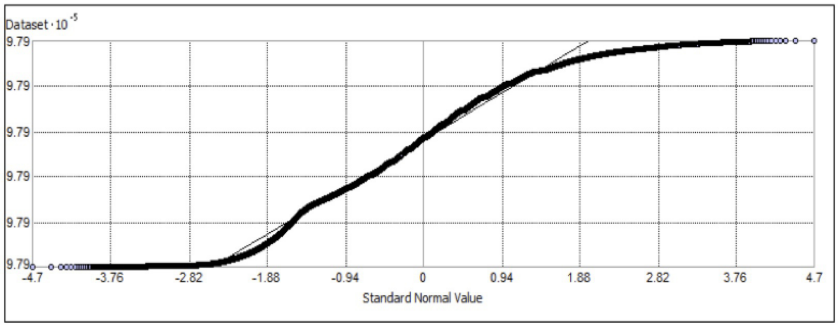

Figure 9: Normal QQ plot of gravity on the ellipsoid data (unit in mgal).

3 Kriging of gravity on the geoid

The kriging method here was conducted in ArcGIS 10.1, which includes semivariogram modeling, searching neighborhood, and cross validation. The central tool of Geostatistics is the variogram/semivariogram, which summarizes the spatial autocorrelation. Cross validation is assessing how well the kriging method predicts.

There are six types of kriging in Geostatistical Analyst tools of ArcGIS 10.1. The most common types are ordinary kriging and universal kriging, which were chosen to be used in this paper. The simple kriging method is also quite common, but it requires the data to have a normal distribution. Thus, the simple kriging method was not used in this paper.

3.1 Ordinary kriging of gravity on the geoid

The nugget, the range and the partial sill of the semivariogram were compared between the stable technique and the Gaussian technique of the ordinary kriging. There is no difference between the stable technique and the Gaussian technique of the ordinary kriging of gravity on the geoid (Table 2). In this case, the semivariogram displaced in Figures 10 to 13 stands for both stable and Gaussian techniques, and the model "perfect" fit through the averaged binned values at the distance h.

Table 2: Comparison of the components of stable and Gaussian semivariogram (units of nugget, partial sill and sill are mgal^2; unit of range is degree).

Type	Nugget	Range	Partial Sill	Sill
Stable	28.12	5.52	16437.37	16465.49
Gaussian	28.12	5.52	16437.37	16465.49

The predicted, error, standard error, and normal QQ plot graphs are plotted respectively in Figure 14 (A to D). The predicted graph shows how well the known sample value was predicted compared to its actual value. The regression function in Figure 14A is $f(x) = 0.9999x + 125.1751$. By visually analyzing the graph, the regression function is closely aligned with the reference line. Therefore, it is well predicted.

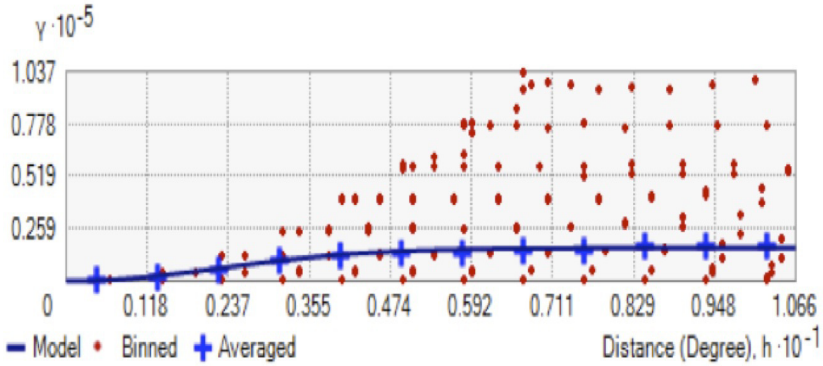

Figure 10: Semivariogram model of the ordinary kriging. The averaged semivariogram values on the y-axis $\left(\text{in mgal}^2\right)$, and distance (or lag) on the x-axis (in degree). Binned values are shown as red dots, which are sorted the relative values between points based on their distances and directions and computed a value by square of the difference between the original values of points; Average values are shown as blue crosses, which are generated by binning semivariogram points; The model is shown as blue curve, which is fitted to average values. Model: $28.118 \times Nugget + 16437 \times Stable(5.53, 2)$; Model: $28.118 \times Nugget + 16437 \times Gaussian(5.53)$.

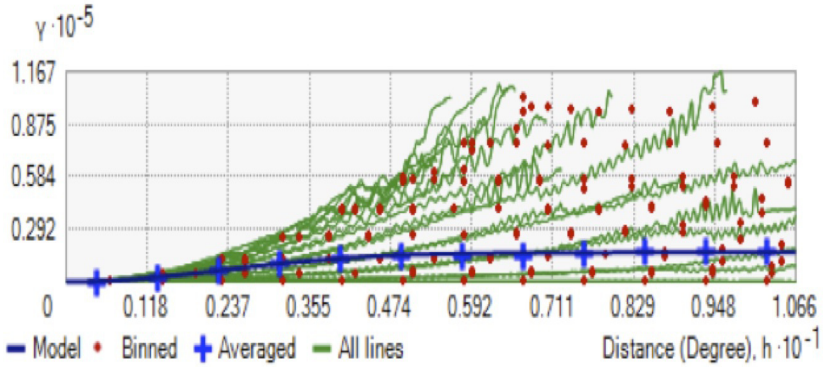

Figure 11: Semivariogram with all lines (green lines) which fit binned semivariogram values. The averaged semivariogram values on the y-axis $\left(\text{in mgal}^2\right)$, and distance (or lag) on the x-axis (in degree).

The error graph shows the difference between known values and predictions for these values. The error equation in Figure 14B is $y = -0.0001x + 125.1751$. The standardized error graph shows the error divided by the

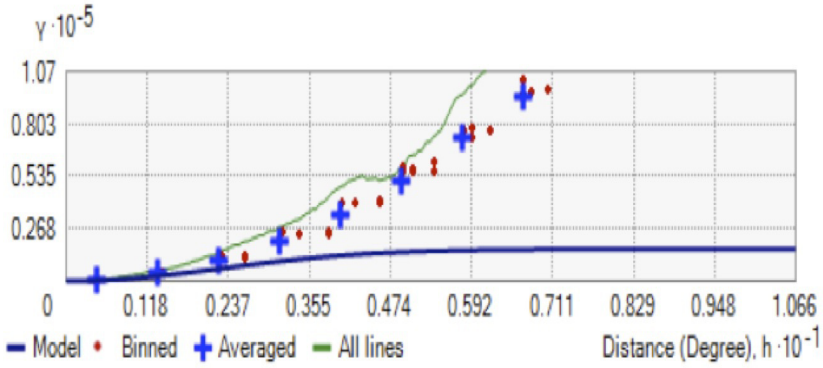

Figure 12: Semivariogram with showing search direction. The tolerance is 45 and the bandwidth (lags) is 3. The local polynomial shown as a green line fits the semivariogram surface in this case. The averaged semivariogram values on the y-axis $\left(\text{in mgal}^2\right)$, and distance (or lag) on the x-axis (in degree).

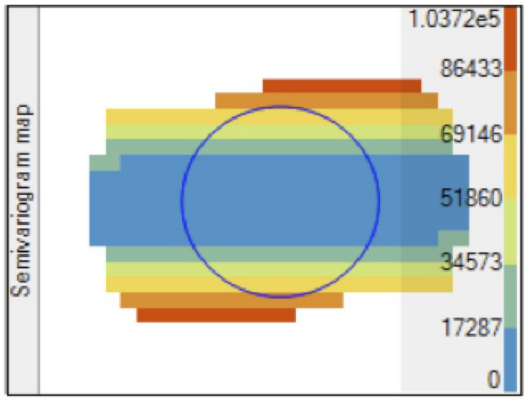

Figure 13: A semivariogram map. The color band shows semivariogram values with weights $\left(\text{unit in mgal}^2\right)$.

estimated kriging errors. The standardized error equation in Figure 14C is $y = -0.00002x + 22.9974$. The normal QQ plot of the standardized error (Figure 14D) shows how closely the difference between the errors of predicted and actual values align with the standard normal distribution (the reference line). Figure 15 to Figure 18 displace the prediction and standard error map by using the ordinary kriging with stable and Gaussian techniques.

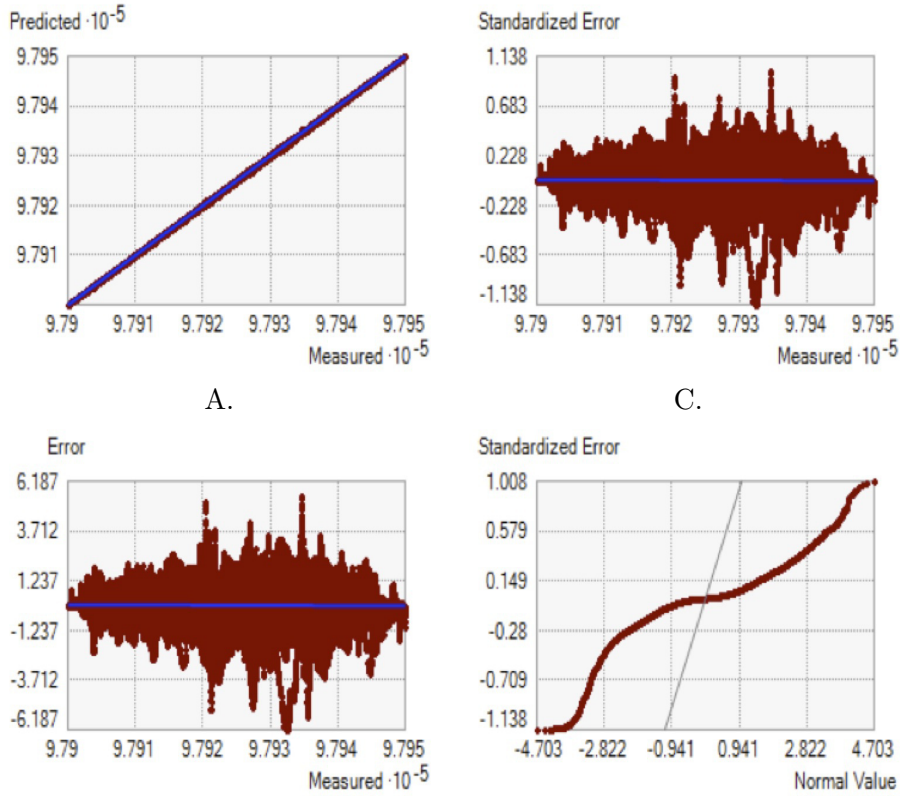

Figure 14: Cross validation of the ordinary kriging (unit in mgal). A. The predicted graph. The blue line represents the regression function, and the black line represents the reference line; B. The error graph. The blue line represents the error equation; C. The standardized error graph. The blue line represents the standardized error equation; D. The normal QQ plot of the standardized error. The reference line is represented by the black line.

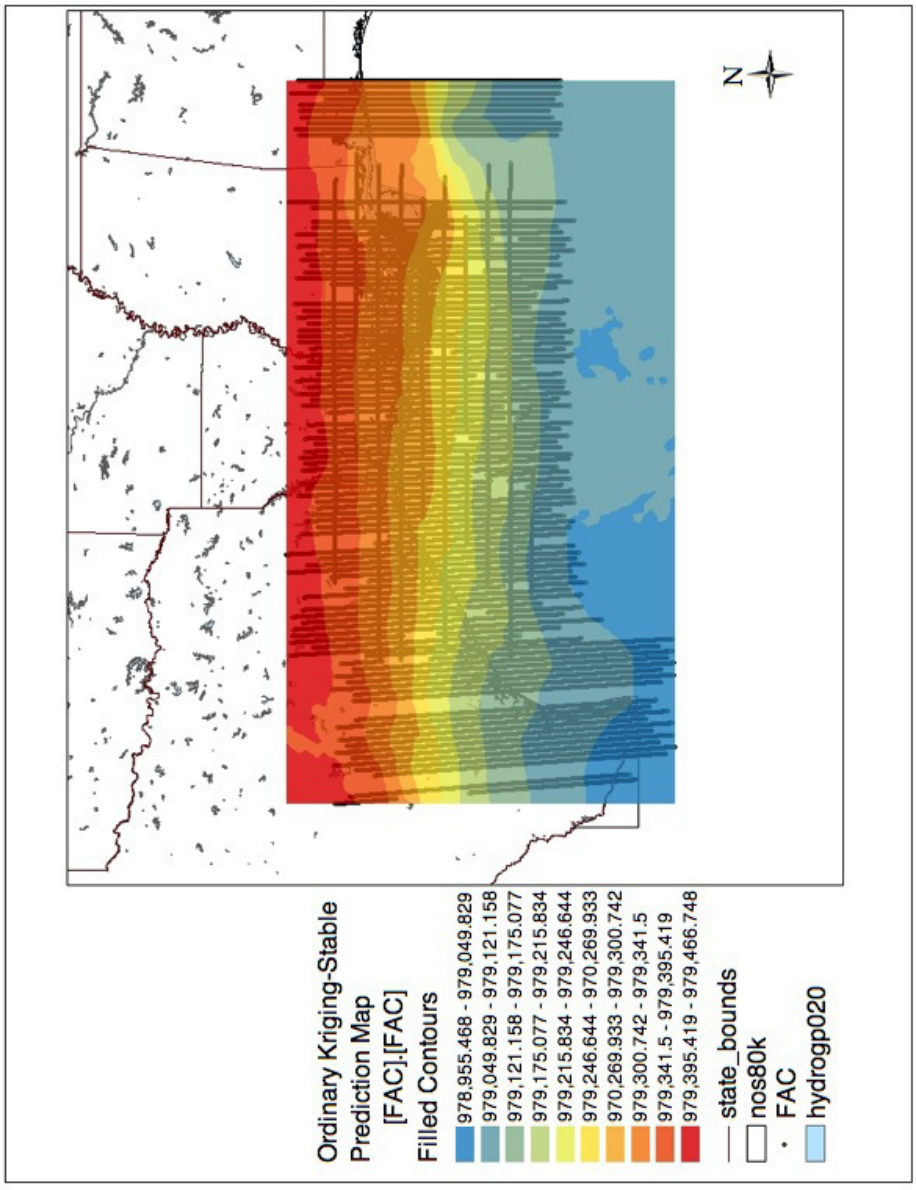

Figure 15: The ordinary stable kriging predictions map (unit in mgal).

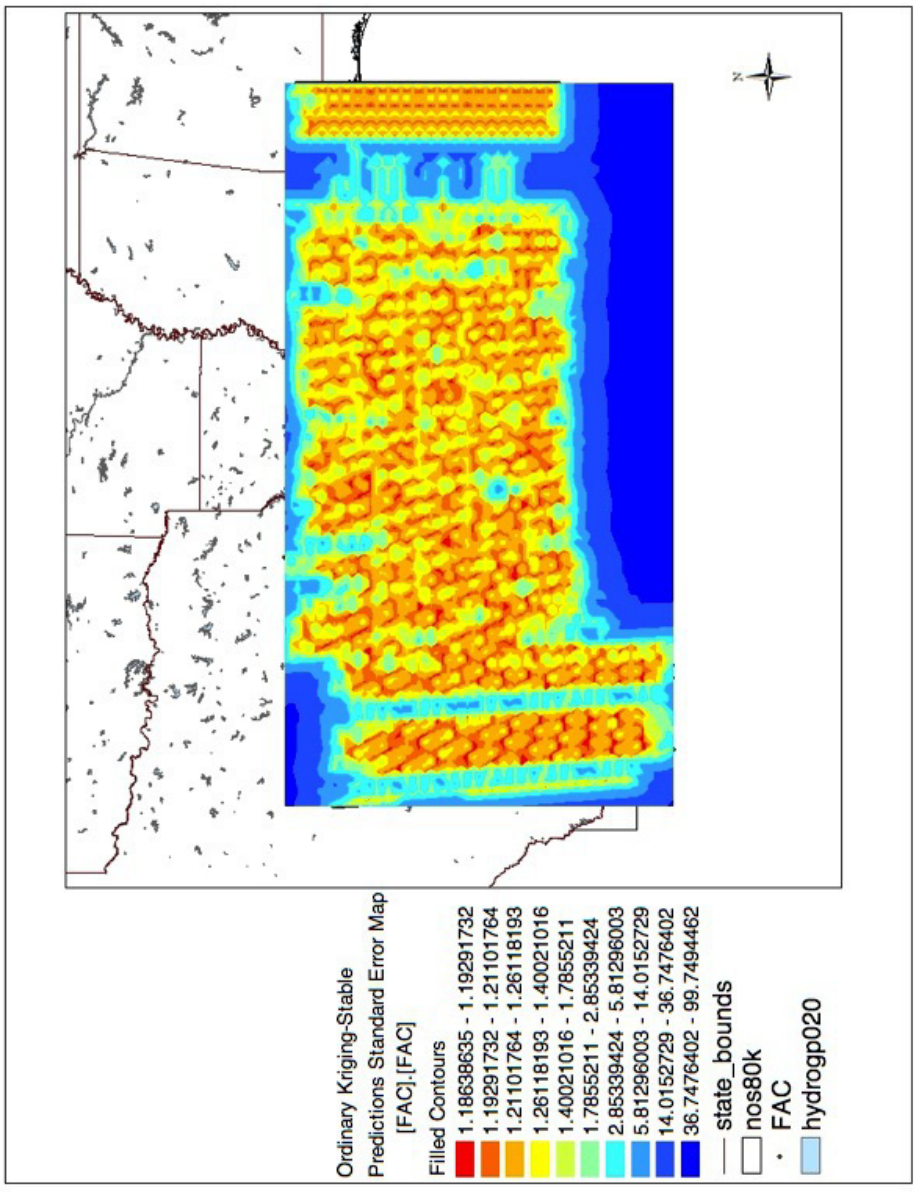

Figure 16: The ordinary stable kriging prediction standard error map (unit in mgal).

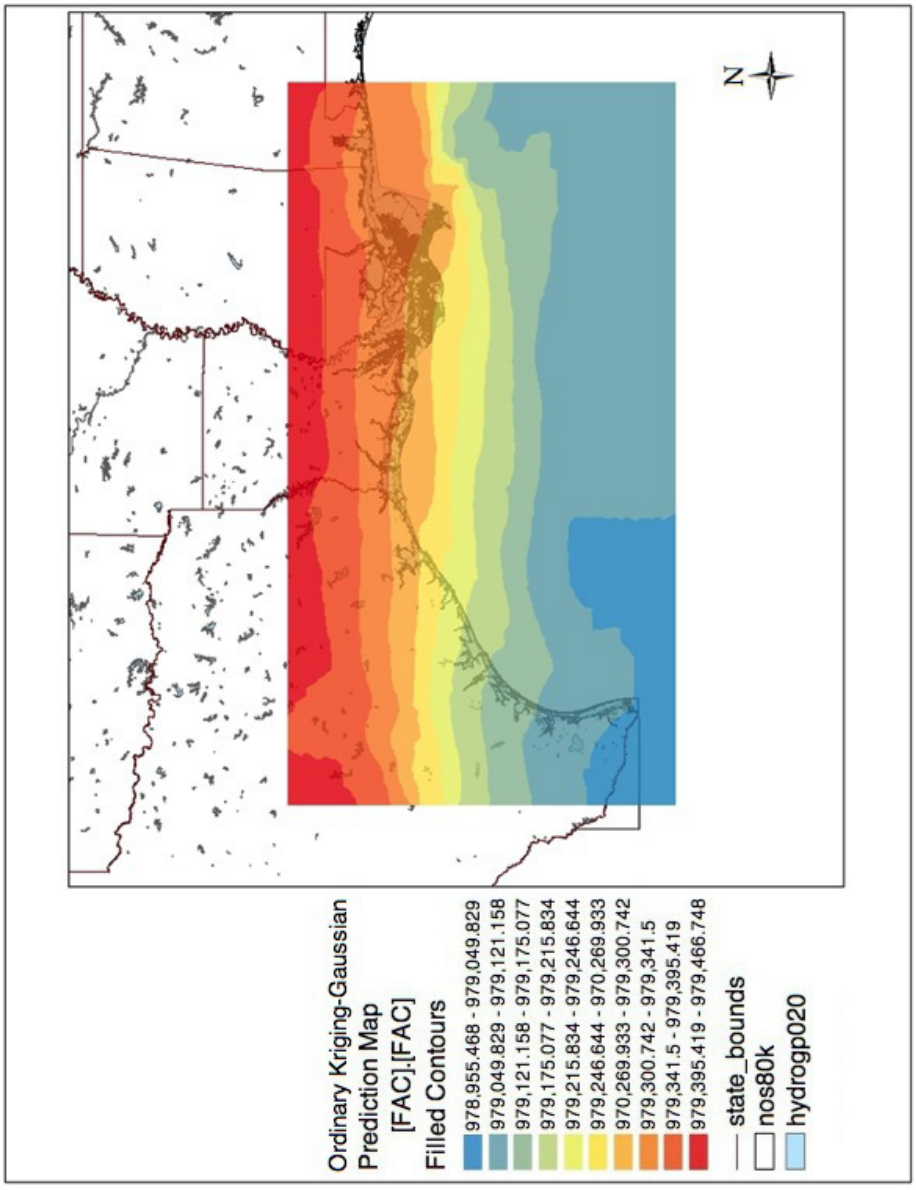

Figure 17: The ordinary Gaussian kriging predictions map (unit in mgal).

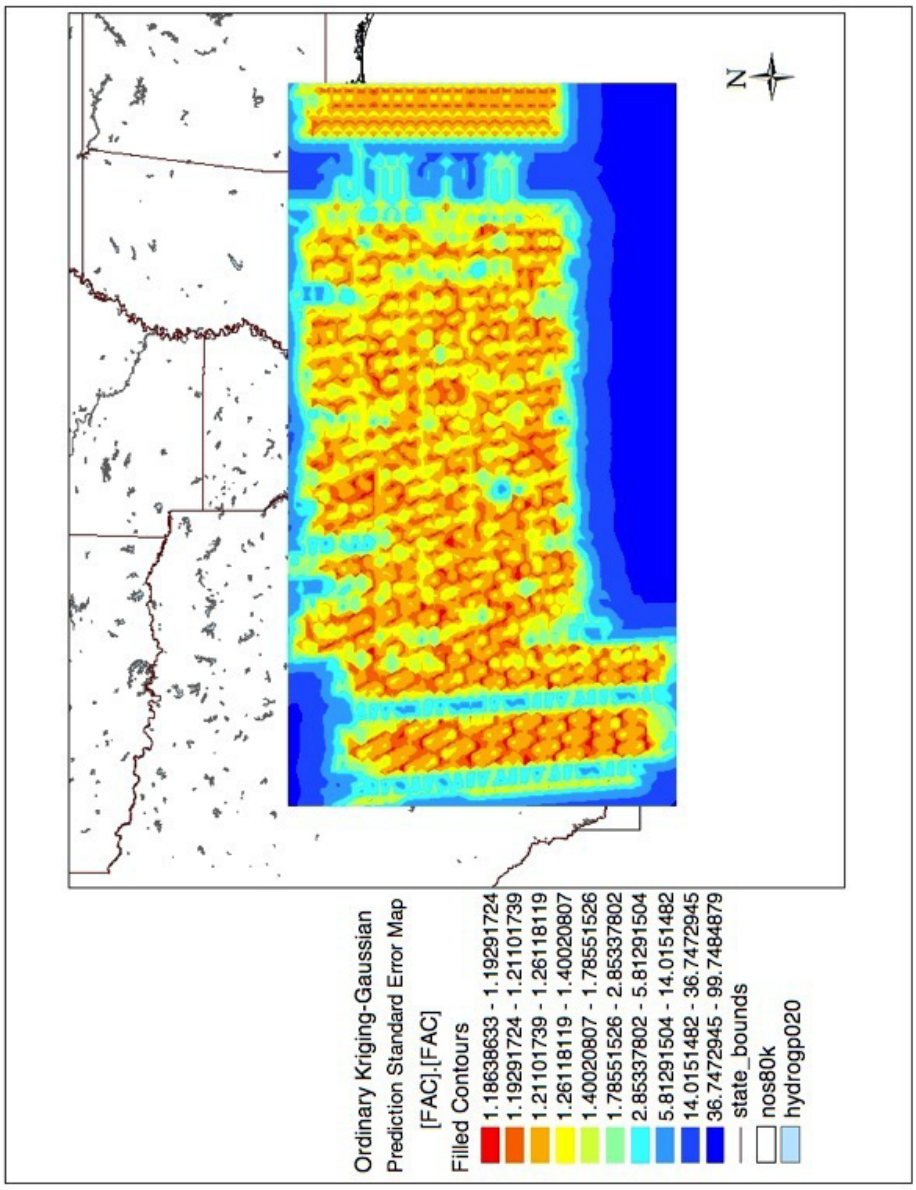

Figure 18: The ordinary Gaussian kriging prediction standard error map (unit in mgal).

3.2 Universal kriging of gravity on the geoid

Trend analysis was presented in Figure 19. There is no trend because the curve through the projected points is flat (as shown by the light blue line in the Figure 19). A slight downward curve as shown by the red line in Figure 19 is through the projected points on ZY plane, which suggests that there may be a trend existing in the gravity-on-the-geoid data. Therefore, de-trend is conducted before the universal kriging process in order to prevent biases in the analysis. Because the curve shown on ZY plane is not obvious, the de-trend approach is chosen to remove the trend order as constant. The process was conducted in ArcGIS 10.1 by using Geostatistical Analyst. Results of the universal kriging with either the stable technique or the Gaussian technique were shown to have the exact same as results of the ordinary kriging.

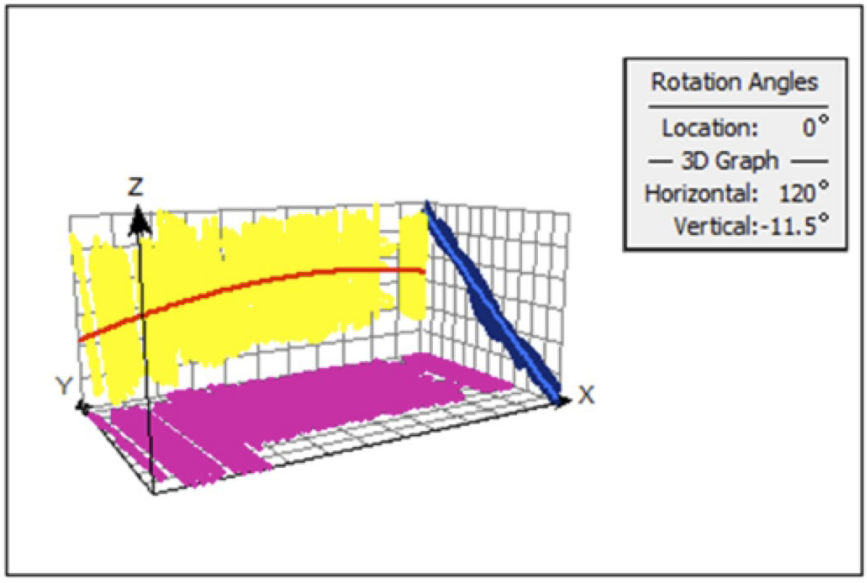

Figure 19: Trend analysis of gravity on the geoid. Legend: Grid (XYZ): Number of Grid Lines 11×11×6; Projected Data: YZ plane (Dark Blue), ZY plane (Yellow), XY plane (Peony Pink); Trend on Projections: YZ plane (Light Blue), XZ plane (Red); Axes (Black).

3.3 Results and evaluation of error

A better interpolation method should have a smaller RMS. Due to no difference between the ordinary kriging and universal kriging in this case; statistical results were the same as those listed in Table 3. The prediction error mean is 0.0038 mgal. As 1 meter increased in altitude, the gravity is decreased by 0.3086 mgal. With simple conversion, the accuracy of prediction is approximately 0.0123 meters. Namely, it is around 1.23 cm, which is close to expectations.

Table 3: Statistics (unit in mgal).

RMS Standardize	0.1084
Mean Standardize	0.0007
Average Standard Error (ASE)	5.5060
Root Mean Square (RMS)	0.5918
Difference between RMS and ASE	4.9142
Difference in Percentage	89.25%

4 Kriging of difference between gravity on the ellipsoid and the geoid

The kriging method used in this section is the ordinary kriging with the stable technique. The nugget in semivariogram (Figures 20 to 22) is approximately 1.0324 mgal^2, which is very small. The range is 2.2212 degree, and the partial sill is 355.2671 mgal^2. Figure 23 is an example of a semivariogram map with weight values.

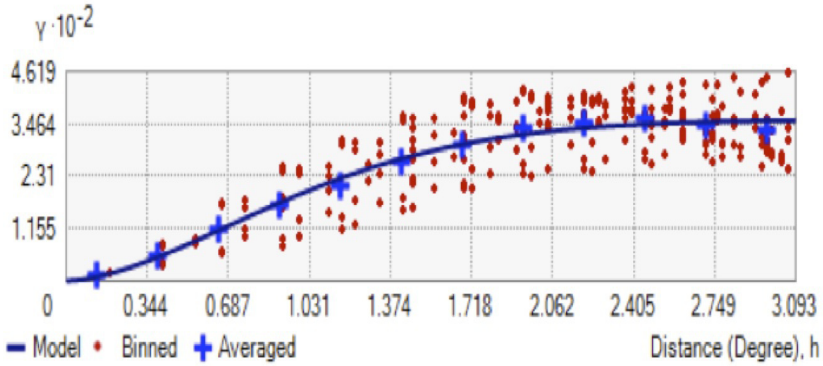

Figure 20: Semivariogram model of the ordinary kriging. The averaged semivariogram values on the y-axis $\left(\text{in mgal}^2\right)$, and distance (or lag) on the x-axis (in degree). Binned values are shown as red dots, which are sorted the relative values between points based on their distances and directions and computed a value by square of the difference between the original values of points; Average values are shown as blue crosses, which are generated by binning semivariogram points; The model is shown as blue curve, which is fitted to average values. Model: $1.0324 \times Nugget + 355.27 \times Stable(2.2212, 1.6818)$.

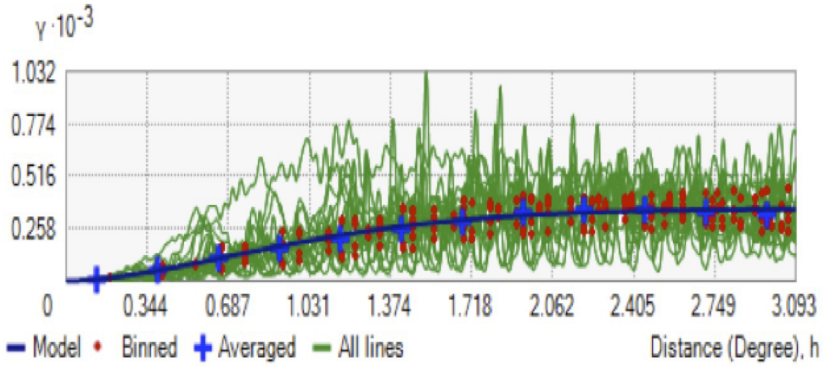

Figure 21: Semivariogram with all lines (green lines) which fit binned semivariogram values. The averaged semivariogram values on the y-axis $\left(\text{in mgal}^2\right)$, and distance (or lag) on the x-axis (in degree).

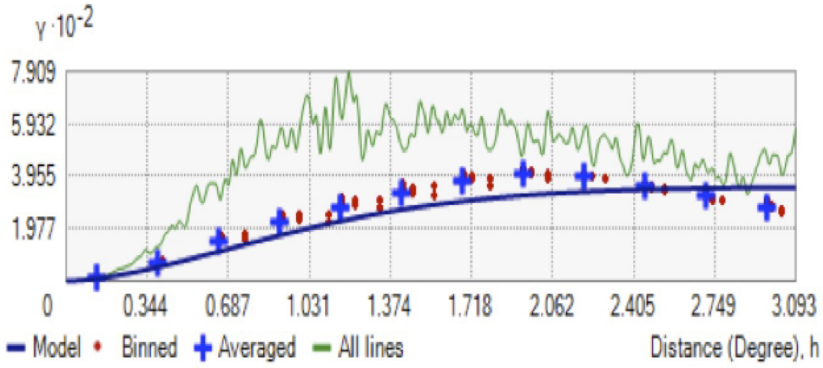

Figure 22: Semivariogram with showing search direction. The tolerance is 45 and the bandwidth (lags) is 3. The local polynomial shown as a green line fits the semivariogram surface in this case. The averaged semivariogram values on the y-axis $\left(\text{in mgal}^2\right)$, and distance (or lag) on the x-axis (in degree).

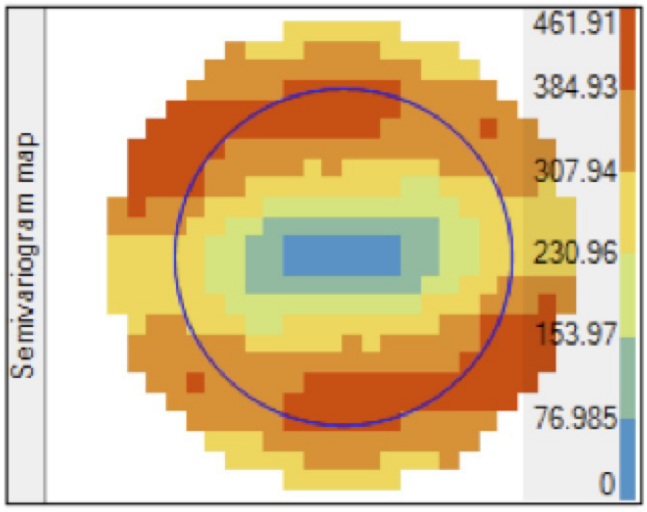

Figure 23: A semivariogram map. The color band shows semivariogram values with weights $\left(\text{unit in mgal}^2\right)$.

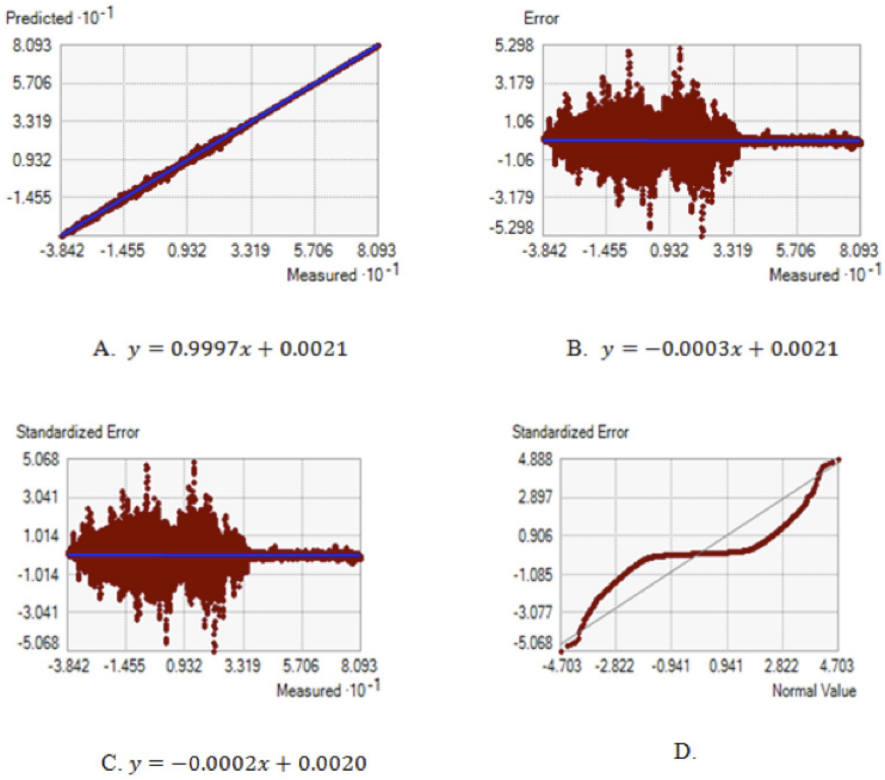

Figure 24: Cross validation of the ordinary kriging (unit in mgal).

The predicted, error, standard error, and normal QQ plot graphs are plotted respectively in Figure 24 (A to D). Statistical results of the ordinary kriging of difference between gravity on the ellipsoid and the geoid listed in Table 4. The prediction yields very small RMS. The mean of prediction error is approximately 0.00076 mgal. Figure 25 is the ordinary kriging prediction map which displays the shape of the geoid.

Table 4: Statistics (unit in mgal).

RMS Standardize	0.2249
Mean Standardize	0.0007
Average Standard Error (ASE)	1.0672
Root Mean Square (RMS)	0.2369
Difference between RMS and ASE	0.8303
Difference in Percentage	77.80%

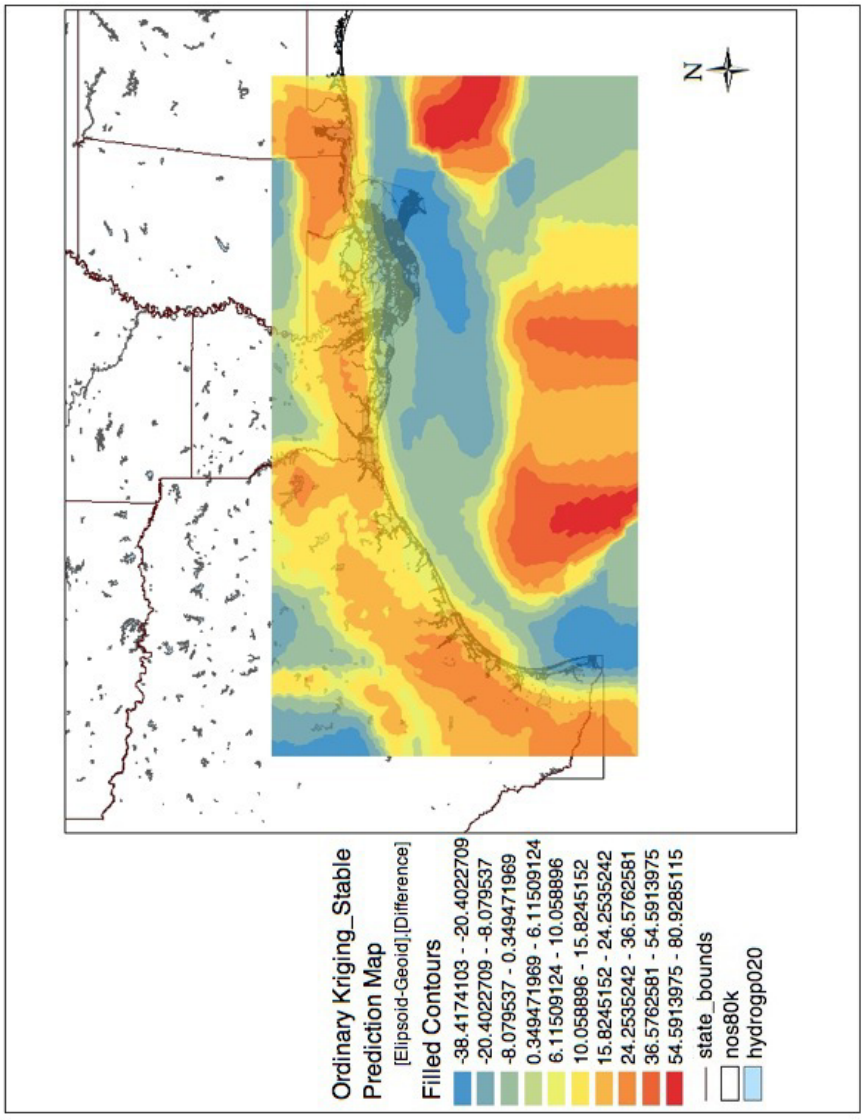

Figure 25: The ordinary kriging predictions map (unit in mgal).

5 Discussion

Geostatistics is a technique that is used to predict unsampled values from observed values accurately. Location of attribute values can be referred as the key of choosing methodology. In this paper, we analyzed four blocks as a group. Thus, a coincident data sample existed in some places. In this case, using average of coincident data sample was applied. This may have a small influence on the kriging process. In a future study, we will analyze four blocks individually. In this paper, we have the mean precision of prediction is around 1.23 cm, which is a very good result for coastal regions.

Acknowledgements

Thanks to NGS at NOAA for open access to download GRAV-D airborne gravity data. For more information and project materials [1, 2, 3, 4, 5], visit NGS on the Web (GRAV-D Homepage: `http://www.ngs.noaa.gov/GRAV-D`). Other file data used in the map (named as nos80k, state_bounds, hydrogp020) was download from USGS [9, 10, 12].

References

[1] Damiani, T.M. (Ed.) (2011) "GRAV-D General Airborne Gravity Data User Manual". Theresa M. Diehl, ed., Version 1. GRAV-D Science Team. `http://www.ngs.noaa.gov/GRAV-D/data/NGS_GRAV-D_General_Airborne_Gravity_Data_User_Manual_v1.1.pdf`, accessed 04/19/2012.

[2] GRAV-D Science Team (2011) "Gravity for the Redefinition of the American Vertical Datum (GRAV-D) Project, Airborne Gravity Data; Block CS01". In: `http://www.ngs.noaa.gov/GRAV-D/data_cs01.shtml`, accessed 04/19/2012.

[3] GRAV-D Science Team (2011) "Gravity for the Redefinition of the American Vertical Datum (GRAV-D) Project, Airborne Gravity Data; Block CS04". In: `http://www.ngs.noaa.gov/GRAV-D/data_cs04.shtml`, accessed 04/19/2012.

[4] GRAV-D Science Team (2012) "Gravity for the Redefinition of the American Vertical Datum (GRAV-D) Project, Airborne Gravity

Data; Block CS02". In: http://www.ngs.noaa.gov/GRAV-D/data_cs02.shtml, accessed 04/19/2012.

[5] GRAV-D Science Team (2012) "Gravity for the Redefinition of the American Vertical Datum (GRAV-D) Project, Airborne Gravity Data; Block CS03". In: http://www.ngs.noaa.gov/GRAV-D/data_cs03.shtml, accessed 04/19/2012.

[6] Hofmann-Wellenhof, B.; Moritz, H. (2006) *Physical Geodesy (2nd ed.)*. Springer, Wien, New York.

[7] Li, X.; Götze, H.J. (2001) "Tutorial ellipsoid, geoid, gravity, geodesy, and geophysics", *Geophysics* **66**(6): 1660–1668.

[8] Moritz, H. (1980) "Geodetic reference system 1980", *Journal of Geodesy* **54**(3): 395–405.

[9] National Oceanic and Atmospheric Administration (NOAA); National Ocean Service (NOS); Office of Coast Survey; Strategic Environmental Assessments (SEA); Division of the Office of Ocean Resources Conservation and Assessment (ORCA) (1994) "NOS80K - Medium Resolution Digital Vector U.S. Shoreline shapefile for the contiguous United States". In: http://coastalmap.marine.usgs.gov/GISdata/basemaps/coastlines/nos80k/nos80k.zip, accessed 01/19/2012.

[10] Paskevich, V. (2005) "STATE_BOUNDS: internal US state boundaries". In: http://pubs.usgs.gov/of/2005/1071/data/background/us_bnds/state_bounds.zip, accessed 01/19/2012.

[11] Reguzzoni, M.; Sansó, F.; Venuti, G. (2005) "The theory of general kriging, with applications to the determination of a local geoid", *Geophysical Journal International* **162**(2): 303–314.

[12] U.S. Geological Survey (2003) "HYDROGP020 - U.S. National Atlas Water Feature Areas: bays, glaciers, lakes and swamps". In: http://coastalmap.marine.usgs.gov/GISdata/basemaps/usa/water/hydrogp020.zip, accessed 01/19/2012.